

# Novel strategies for complex foothills seismic imaging — Part 1: Mega-near-surface velocity estimation

Yalin Li<sup>1</sup>, Xianhuai Zhu<sup>2</sup>, Gengxin Peng<sup>1</sup>, Liansheng Liu<sup>3</sup>, and Wensheng Duan<sup>1</sup>

## Abstract

Seismic imaging in foothills areas is challenging because of the complexity of the near-surface and subsurface structures. Single seismic surveys often are not adequate in a foothill-exploration area, and multiple phases with different acquisition designs within the same block are required over time to get desired sampling in space and azimuths for optimizing noise attenuation, velocity estimation, and migration. This is partly because of economic concerns, and it is partly because technology is progressing over time, creating the need for unified criteria in processing workflows and parameters at different blocks in a study area. Each block is defined as a function of not only location but also the acquisition and processing phase. An innovative idea for complex foothills seismic imaging is presented to solve a matrix of blocks and tasks. For each task, such as near-surface velocity estimation and static corrections, signal processing, prestack time migration, velocity-model building, and prestack depth migration, one or two best service companies are selected to work on all blocks. We have implemented streamlined processing efficiently so that Task-1 to Task-n progressed with good coordination. Application of this innovative approach to a mega-project containing 16 3D surveys covering more than 9000 km<sup>2</sup> in the Kelasu foothills, northwestern China, has demonstrated that this innovative approach is a current best practice in complex foothills imaging. To date, this is the largest foothills imaging project in the world. The case study in Kelasu successfully has delivered near-surface velocity models using first arrivals picked up to 3500 m offset for static corrections and 9000 m offset for prestack depth migration from topography. Most importantly, the present megaproject is a merge of several 3D surveys, with the merge performed in a coordinated, systematic fashion in contrast to most land megaprojects. The benefits of this approach and the strategies used in processing data from the various subsurveys are significant. The main achievement from the case study is that the depth images, after the application of the near-surface velocity model estimated from the mega-surveys, are more continuous and geologically plausible, leading to more accurate seismic interpretation.

## Introduction

Seismic exploration and development in foothills regions are attractive because there are good trap conditions for oil and gas accumulations. However, because of the complexity of the near-surface and subsurface structures, seismic acquisition and imaging are difficult in foothills regions.

Figure 1 shows a seismic field crew collecting data across the foothills in the Kuqa Depression of the Tarim Basin, northwestern China (Figure 2). Near-surface conditions are complicated with steep-dip outcrops, Gobi, and farmland (Figure 3). In areas such as Kuqa in China and the Andes foothills in South America, these types of terrain mean that receiver lines will be far apart and there might not even be well-defined shot lines. In addition, planting geophones, or groups of geophones, on

rocky outcrop or dense undercover will be a problem. With such surface sampling, it is hard to sample the slow noise enough to attack it using standard methods. Also, it is extremely difficult to apply advanced imaging such as reverse time migration, which needs fine crossline spacing especially at high frequencies (Gray and Zhu, 2019).

Dense, wide-azimuth seismic surveys usually are carried out over time with different acquisition stages within a foothills-exploration area. This involves considerably more surface effort than standard one-time wide azimuth acquisition. Because of the complexity in the near surface and subsurface, it is hard to acquire with receiver lines along strike, then dip, and then intermediate in foothills settings. Very often, a full-azimuth survey is composed of two or more wide-azimuth surveys with a certain overlap. This is necessary and practical in

<sup>1</sup>Tarim Oilfield Company, PetroChina, Korla 841000, China. E-mail: liyal\_sc@cnpc.com.cn; penggx-tlm@petrochina.com.cn; dws-tlm@petrochina.com.cn.

<sup>2</sup>Forland Geophysical Services (FGS), Houston 77079, USA. E-mail: xzhu@forlandgeo.com (corresponding author).

<sup>3</sup>PanImaging, Beijing 100086, China. E-mail: liu@panimaging.com.

Manuscript received by the Editor 22 September 2019; revised manuscript received 25 April 2020; published ahead of production 11 June 2020; published online 1 July 2020. This paper appears in *Interpretation*, Vol. 8, No. 3 (August 2020); p. T651–T665, 28 FIGS.

<http://dx.doi.org/10.1190/INT-2019-0204.1>. © 2020 Society of Exploration Geophysicists and American Association of Petroleum Geologists. All rights reserved.

foothills exploration, partly because of the economic concerns. In this scenario, determining how to set up unified criteria for processing workflows and parameters at different blocks in a study area is critical. Here, each



**Figure 1.** Foothills exploration is challenging. This is a field crew collecting seismic data across the foothills in the Kuqa Depression of the Tarim Basin, northwestern China. (Source: <https://finance.sina.com.cn/roll/2019-06-25/doc-ihyt-cerk9063950.shtml>.)

block is defined as a function of not only location but also of time for seismic acquisition. Multiple acquisition and processing phases involving, for example, wider azimuths and denser receivers, usually are needed at specific blocks in foothills areas for improved structural imaging and reservoir characterization.

Figure 4 shows a matrix of blocks and tasks. The blocks (Block-I, Block-II, . . . , Block-N) in the horizontal direction represent geophysical operations in space and time, meaning that a task can take place at a specific location with different times or phases. Each block refers to a single portion of the entire survey; for example, KeShen 3D in Figure 3. Tasks (Task-I, Task-II, . . . , Task-M) in the vertical direction illustrate geophysical milestones such as near-surface velocity estimation and statics, signal processing and stack, prestack time migration (PSTM), velocity model building and prestack depth migration (PSDM), and seismic inversion. For consistency, unified criteria across all blocks are required for each task. Figure 5a shows an example of nine unified criteria for task-1: near-surface velocity estimation and statics. The base of the weathered layer (Figure 5b, modified from Taner et al., 2007) also is frequently called the “top of a high-velocity refraction layer,” which is to be defined in calculating statics.

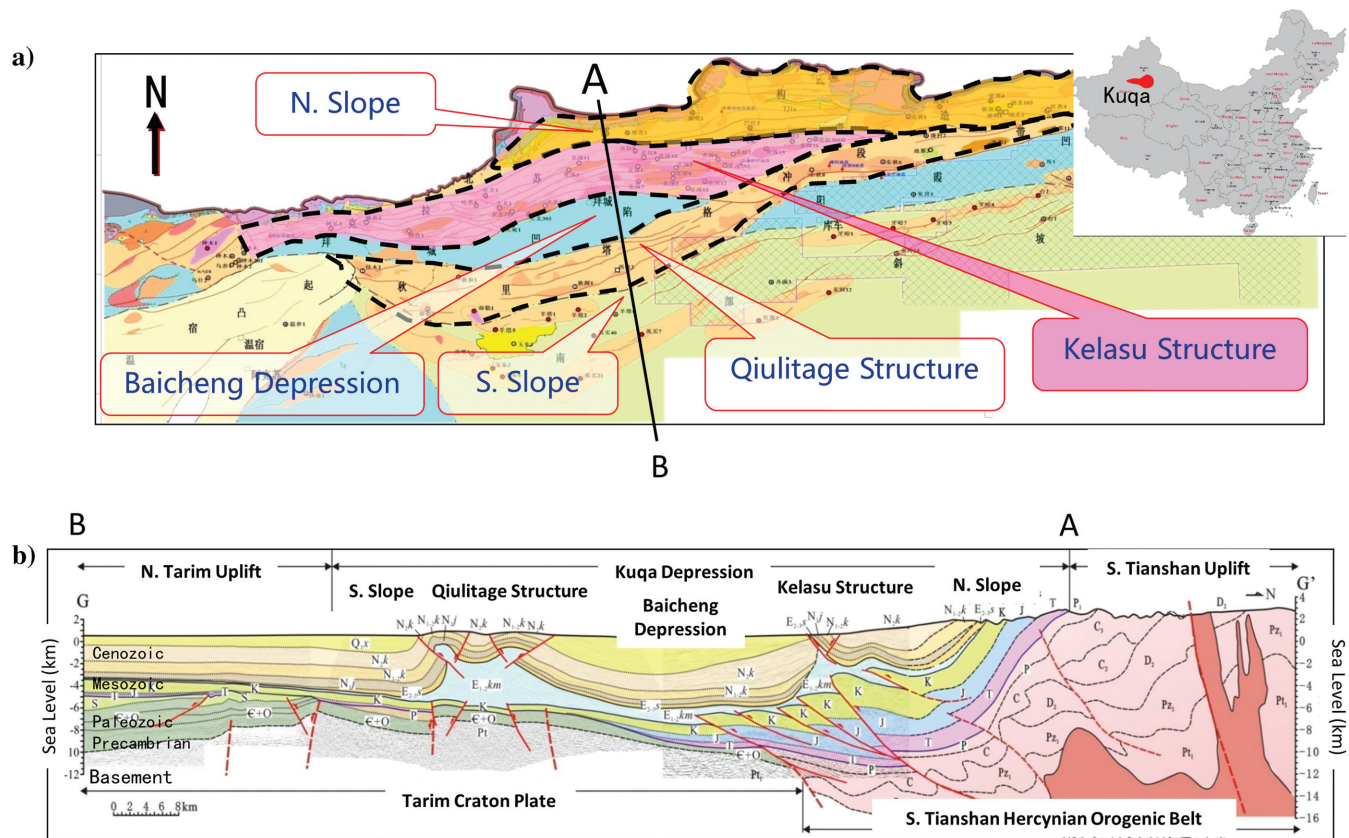


**Figure 2.** Regional geology across Kuqa Depression of Tarim Basin, northwestern China. (a) Kelasu, Qiulitage, and Northern Slope are three major structures in the Kuqa Depression, and Kelasu has the most gas reserves, more than 50% of the Tarim oilfield. (b) A regional geologic cross section A-B in (a), from the South-Tianshan Mountain uplift in the north to the Kuqa Depression in the middle, and the North-Tarim uplift in the south. Reverse faults caused by the tectonic movement of Tianshan Mountain are evident in Kelasu structure of the Kuqa Depression, forming good reservoirs in Cretaceous below a regional cap rock of Paleogene gypsum.

Solving the matrix (Figure 4) is challenging because there is no existing example in geophysics. Based on industrial experience outside the oil and gas industry, we conduct the following strategies and policies:

- 1) A task force is formed within the Tarim Oilfield company (oil company), including the management team members, technical experts, and project leaders. This committee is responsible for coordination and integration of all tasks at different blocks.
- 2) For each task, one or two best service companies are selected from the industry based on their technical expertise, organization stability, and service quality from an open bidding process.
- 3) Quality control is performed by the service companies themselves first for each task and then checked and passed by the oil company and other service companies who are responsible for the next task (Figure 4).
- 4) Each service company is encouraged to set up a local office inside the oil company, and key technical personnel should regularly work on site to ensure the consistency and quality of services.
- 5) Oil company and service companies work together from the beginning of the project, and each service company is assigned a delegated contact person from the oil company.
- 6) Oil company and service companies share some resources, including hardware and software.
- 7) Oil and service companies meet regularly to review the project status and the path forward.

We have applied this approach consistently to the Kelasu-foothills-imaging megaproject.

Foothills seismic acquisition and imaging in most parts of the world (North and South America in particular) have not advanced in the past decade to the degree that marine and arid land (e.g., Arabian Peninsula and North Africa) have. This is because the economics of gas-rich foothills prospects usually are not good. However, external dependence on oil and natural gas in China is increasing. From an environmental protection point of view, natural gas increasingly is being used to replace coal, and the trend will continue. In addition, the price of natural gas relative to that of oil in China is higher than that in North America and most other regions in the world. The Kelasu thrust belt is the most important oil

and gas exploration and production area in the Kuqa Depression of Tarim oilfield, northwestern China. It has favorable petroleum geologic conditions with good source rocks, reservoirs, and cap rocks. In total, 25 local structures with gas discovery have been confirmed in Kelasu, containing >100 TCF of gas, more than 50% of the total reserves of the Tarim oilfield.

One of the challenges of seismic exploration in the Kelasu thrust belt is the complexity of near-surface conditions (Figure 3). The terrain is undulating with strong lateral velocity variations. On the surface, there are not

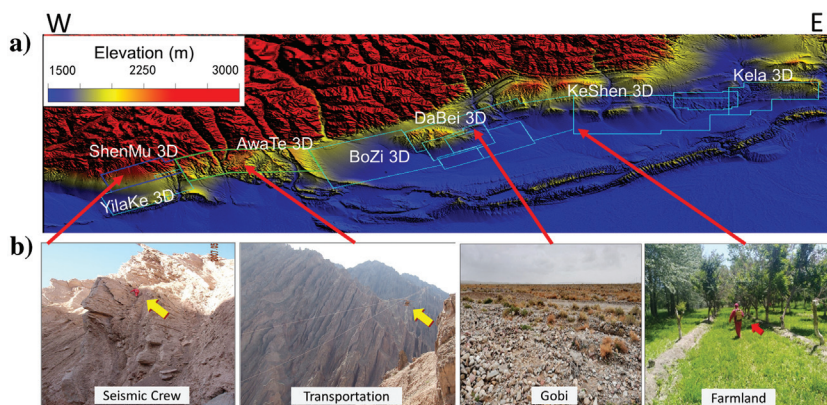


**Figure 3.** Complex near-surface conditions in Kelasu thrust belt in the Kuqa Depression. (a) Elevation changes from 1142–2192 m in KeShen to 1500–3200 m in AwaTe. It is characterized by rough topography and strongly variant near-surface velocities. (b) Field seismic crew operations and equipment transportation are difficult in mountains. Gobi with gravels and farmland with permit issues in (b) also are challenging for seismic acquisition in foothills. Yellow arrows in (b) show geophysicists and equipment in field operation. The first major discovery was in Kela structure (Kela 3D), leading to the forming of the Tarim oilfield.

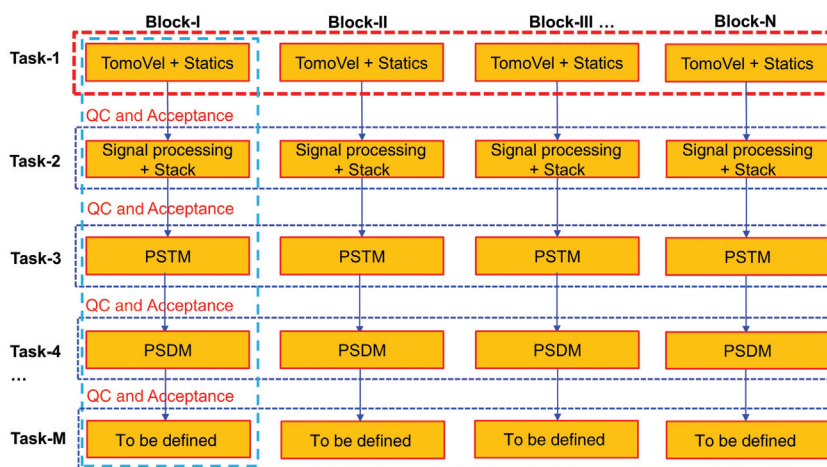


**Figure 4.** A matrix of blocks and tasks. Number of blocks (Block-I, Block-II, ..., Block-N) in horizontal direction represent geophysical operations in space and time. Number of tasks (Task-I, Task-II, ..., Task-M) in vertical direction illustrate geophysical milestones. Each step needs to pass through quality-control checkpoint and then goes to the next step. Normally, the tasks in each block are carried out by a single vendor. However, due to the specialty of E&P in foothills, we implemented an innovative idea to select one or two of the best vendors to perform a specific task at different blocks with the best quality and unified requirements.

only steep hills exposed by high-velocity bedrocks but it is also interleaved with low-velocity gravels and unconsolidated conglomerate rocks formed by alluvial fans (Wang et al., 2013). Beneath the surface, conglomerate rocks in the foreland basin have been episodically deposited and consolidated due to compaction. The thickness of the high-velocity conglomerate rocks varies, typically from tens of meters in KeShen to hundreds of meters in DaBei and several kilometers in BoZi (Figure 3). The high-velocity conglomerate rocks near the surface often cause a velocity reversal, which is problematic for imaging deeper reservoirs (Figures 5b, 6, and 7).

Figure 6a shows that the near-surface high-velocity conglomerate rocks can cause mispositioning of deep targets in the KeShen 12 structure (KS12) of the northeast Kelasu thrust belt (Tian et al., 2018). Well KS12 previously was drilled based on the structural high of legacy PSDM images. Unfortunately, no gas was found, only water. After reprocessing with (1) high-resolution near-surface velocity estimation using turning-ray tomography and tomostatics (Zhu et al., 1992), (2) followed by a joint or integrated refraction and reflection tomography approach (Zhu et al., 2001, 2003; Zhou et al., 2011; Song et al., 2014; Tian et al., 2018), and (3) through tilted-transverse-anisotropic (TTI) PSDM from the topography, we found that the KS12 well (the yellow line in Figure 6a) was not drilled in the right spot; that is, it was ap-

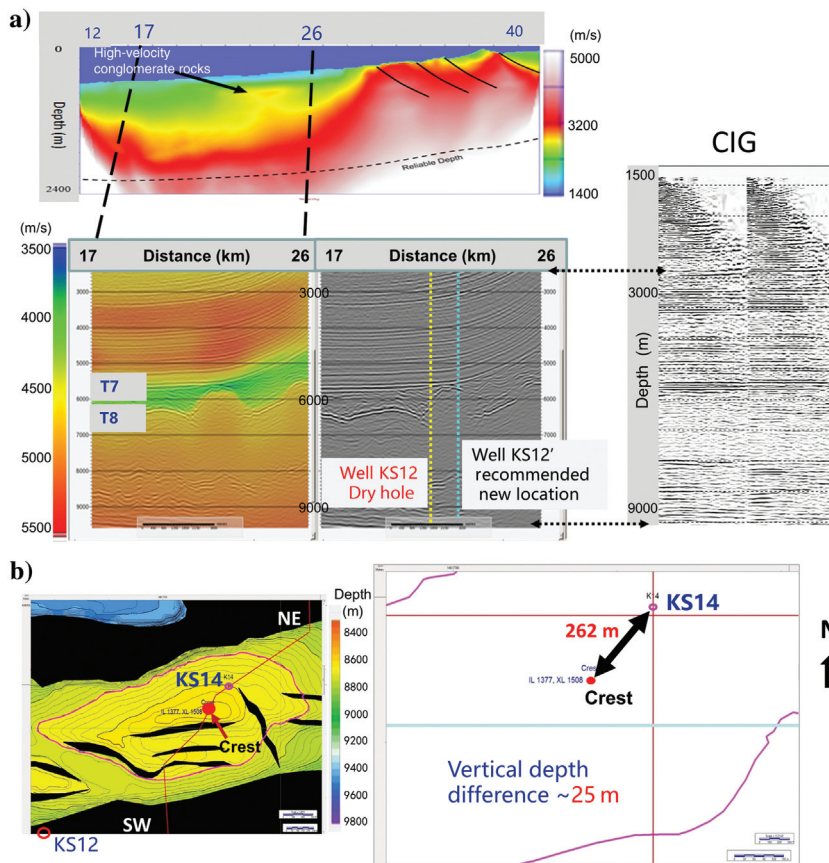


**Figure 6.** (a) Impact of shallow velocities (top) to imaging of deep targets (bottom). The common imaging gather (CIG) is shown on the right. The near-surface velocity model (top left) estimated from turning-ray tomography shows a high-velocity anomaly (arrow) in the foreland basin associated with conglomerate rocks. After TTI PSDM using the near-surface velocity model followed by joint tomography, KS12 well previously drilled was shown to be not on the structural high, approximately 800 m away from the crest. (b) Prediction for well KS14 before entering the target zone. After reprocessing using the near-surface velocity model estimated from turning-ray tomography followed by a joint tomography and TTI PSDM, well KS14 was not drilled on the structural high (Figure 6b, left), approximately 262 m northeast from the crest (Figure 6b, right). However, it was still within the closure. This was confirmed by the drilling program and well testing.

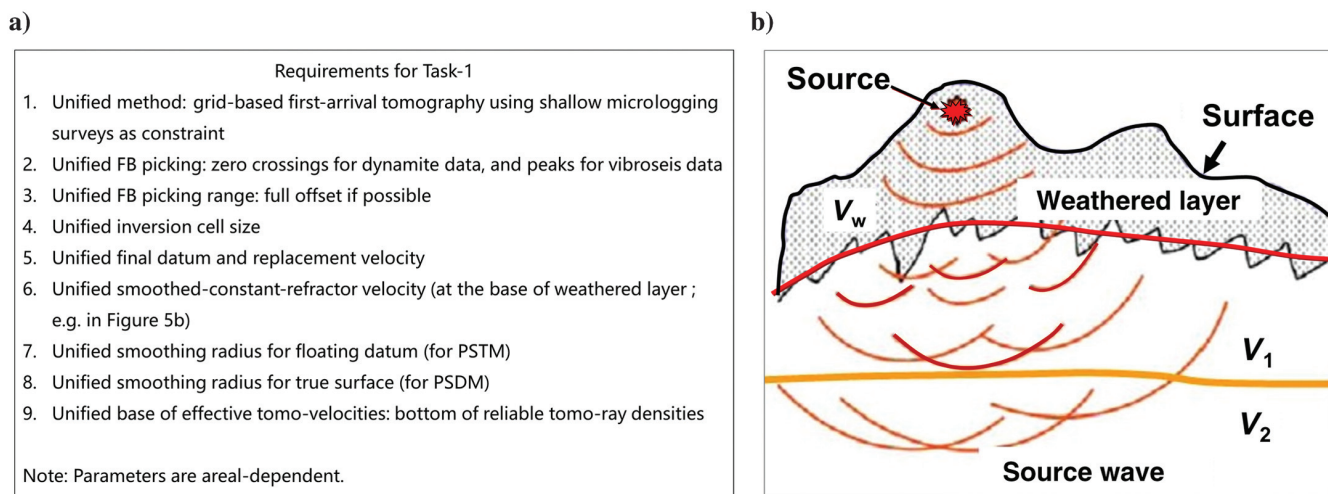


**Figure 5.** (a) Nine unified requirements for task 1: near-surface velocity model estimation and statics. (b) Definition of smoothed-constant-refractor boundary; refractor velocity is equal to  $V_1$ . The weathering velocity is  $V_w$ . There is a reflector between  $V_1$  and  $V_2$ . (Modified from Taner et al., 2007.)

proximately 800 m away from the crest (the blue line in Figure 6a) of the reprocessed PSDM images.

While the reprocessing for KS12 was continuing, a new well was concurrently being drilled on the KeShen 14 structure (KS14) near KS12, without knowledge of the reprocessing team. There is approximately 1645 m of distance between KS12 and KS14. The oil company did not advise the reprocessing team of the KS14 drilling program because it wanted to check the reprocessing results without any biased information. When the reprocessing was completed, the drill bit was only 200 m away from KS14 target in the vertical direction. Based on the reprocessed PSDM images, KS14 also was mispositioned, approximately 262 m northeast from the crest (Figure 6b). Although the distance is significant, it is still within the closure. This was confirmed later by the KS14 drilling results.

Figure 6 illustrates that near-surface velocities play an important role in imaging deeper targets. This is further demonstrated in Figure 7 near KS12 and KS14, where the deep targets below 8000 m are much improved after reprocessing with the near-surface velocities estimated from tomography. The basement below 10,000 m (marked by the arrows in Figure 7) shows a simpler and better focused structure. This is consistent with geologic interpretation.

Given the background and motivation above, Tarim Oilfield Company formed a task force in early 2019 to conduct a mega-seismic-imaging project in the Kela thrust belt, using 16 3D surveys more than 9000 km<sup>2</sup>, including Kela, KeShen, DaBei, BoZi, and AwaTe (Figure 3). This task force was assigned to conduct imaging for three blocks (Kela and KeShen; KeShen and DaBei; and BoZi and AwaTe) for four tasks (Figure 4): (1) near-surface velocity estimation using turning-ray or diving-wave tomography (DWT) for static corrections and velocity-model building, using the first arrivals picked at all offsets if possible, (2) signal processing and stacking, (3) PSTM, and (4) PSDM. To our knowledge, this is the largest and most efficient seismic imaging project to date on foothills areas in the world with significant streamlining and integration processes. The procedures and results presented in this paper could be useful for other foothills areas that require higher surface effort, such as those in North Africa and the Arabian Peninsula.

In the next sections, we will focus on results and illustrations from task-1 of the project: near-surface velocity model building and statics. The results from other tasks will be presented and discussed in separate papers.

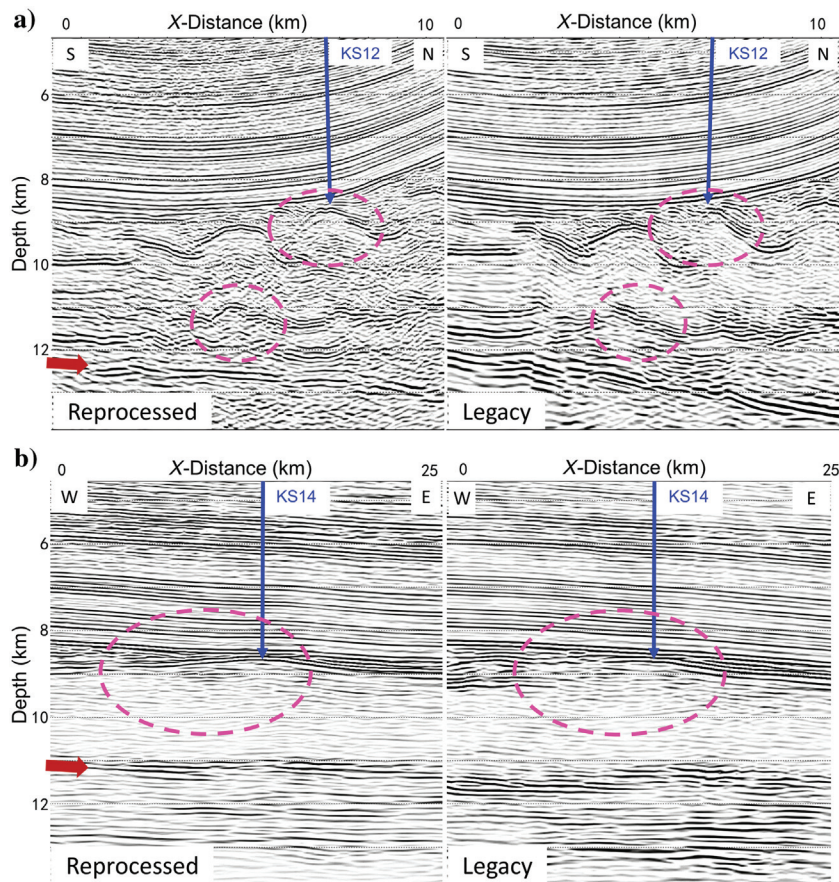


**Figure 7.** (a) A comparison between legacy and reprocessed PSDM for a representative inline near KS12 and KS14. (b) A comparison between legacy and reprocessed PSDM for a representative crossline near KS12 and KS14.

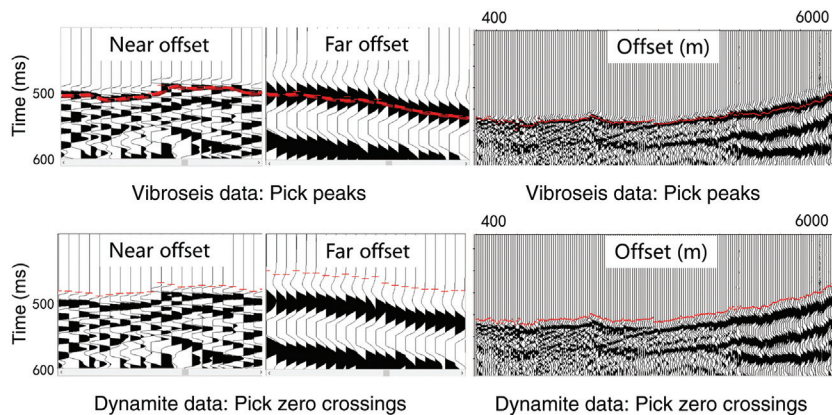


**Figure 8.** First-arrival picking guidelines. For dynamite data, zero crossings are to be picked assuming that the data are minimum phase; for vibroseis data, peaks are to be picked assuming that the data are zero phase. When the S/N of the first arrivals is low in complex areas, picking zero crossings is not easy. In this scenario, peaks usually are picked first and then shifted back to zero crossings, using a spatially variant statistical approach.

## First-arrival picking

The bottleneck of static corrections and near-surface velocity estimations is picking the first arrivals. In this project, we have developed four methodologies to improve the accuracy and efficiency of the first-arrival picking:

- 1) Picking zero crossings instead of peaks (Figure 8). In theory, it is more accurate to pick zero crossings for the first arrivals of dynamite data, assuming that the

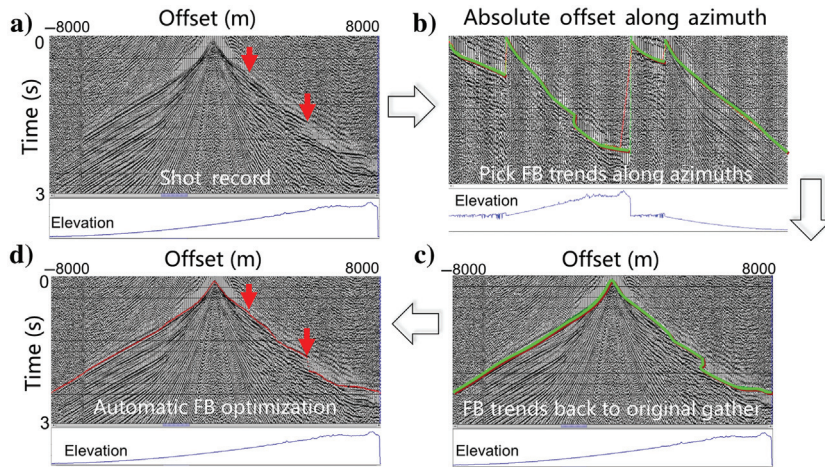


**Figure 9.** A workflow of AI FB picking. (a) A shot record is read in, which usually contains 8–54 cables in the study area. For clarity, only one of the cables is shown in (a); (b) data are sorted into 4–8 different azimuths, and the FB trends or the center lines of the FB windows (green) are picked along the azimuths (using all cables from the same shot record) with the absolute offset increasing in each azimuth. For clarity, only four azimuths are shown in (b); (c) the picked FB trends (green) are displayed back to the original shot record for quality control; and (d) FBs (red) are automatically picked, guided by the windows, using a self-learning approach. Usually, every 20 to 50 shots are selected for autopicking, depending upon the complexity of the near-surface conditions. After autopicking, manual editing is needed, especially in foothills areas.

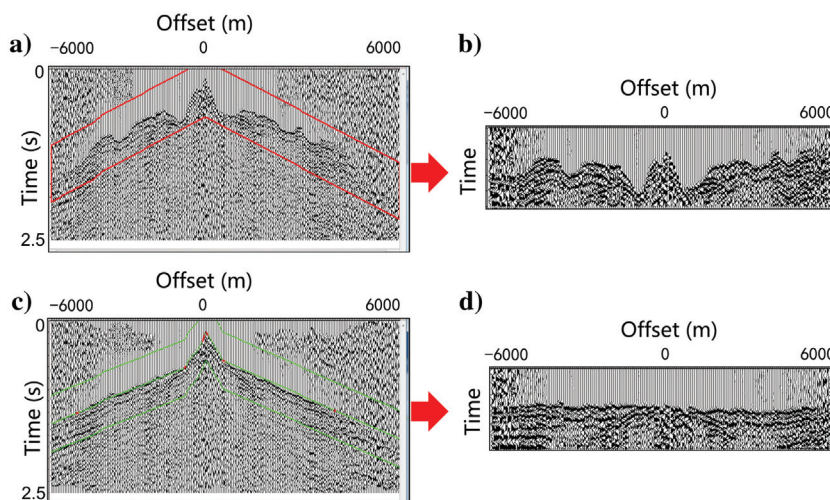


**Figure 10.** Application of spatially variant LMO correction and partial statics before picking and modifying the FBs. (a) An original shot record with a window for the first arrivals, (b) a fixed LMO correction was applied to (a), (c) initial statics were applied to (a), and (d) spatially variant LMO was applied to (c).

data are of minimum phase (Cox, 1999). For vibroseis data with a zero phase, we pick the peaks. In practice, however, very often the automatically picked zero crossings cannot follow the up and down shape of the first arrivals, especially in areas where the signal-to-noise ratio (S/N) is lower. In this scenario, we recommend to first pick the peaks of the first arrivals and then to move them to the zero crossings. Because of the frequency variations at near and far offsets and the lithology and attenuation differences near the surface, a statistical approach should be used to estimate time-shift values from peaks to zero crossings at different offsets.

- 2) Picking first-arrivals using an artificial-intelligence (AI) method (Figure 9). This is important for picking the challenged first arrivals such as “shingles” caused by a thin high-velocity layer (Zhu, 2002). First, we select shots, typically every 10–20 shots depending on the complexity of the data in a study area, and then, we divide a shot record, which usually contains 8–54 cables in the Kelasu surveys, into 4–8 azimuthal sectors as a function of the absolute offset; second, we pick the first-arrival trend or the center line of the first-arrival window (the green line in Figure 9) along each azimuth; third, we project the picked center lines of windows back to the original short records for quality control; and finally, we automatically pick the first arrivals along the picked windows using a self-learning approach. Undefined windows between the picked shots will be interpolated.
- 3) Application of spatially variant linear-moveout (LMO) correction and initial statics (Figure 10). The initial statics usually are a combination of elevation statics, statics estimated from shallow-hole refraction surveys, and initial tomostatics estimated in the field, and they are saved in the field seismic survey files as SPS files. LMO frequently is applied when modifying the picked first arrivals. In the Kelasu foothills, because of the rugged topography and strongly variant near-surface velocities, the first arrivals after LMO appear to have step functions and are difficult to modify (Figure 10). After the application of initial static corrections to the LMO data, the picked first arrivals are more continuous and are easier to

modify. The LMO and initial static corrections are removed before output of the first arrivals.

- 4) Application of a shaping filter to vibroseis data (Figure 11). Vibroseis data very often have long-lasting side lobes in waveforms, which make the first-arrival picking difficult. Conventional band-pass filtering cannot effectively reduce the side lobes for picking the first breaks. However, shaping filtering uses a broad-band wavelet (Yu, 1996). The S/N of the waveforms after shaping filtering has been significantly improved (Figure 11), making it easier for picking the first arrivals.

Based on the survey geometry and the picked first arrivals from the 16 3D surveys from the Kelasu thrust belt, we get the (1) receiver density, (2) first-arrival picking percentage, and (3) time-absolute offset of the first arrivals (Figure 12) for quality control. The picked first arrivals are the input data for the turning-ray tomography to estimate the near-surface velocities.

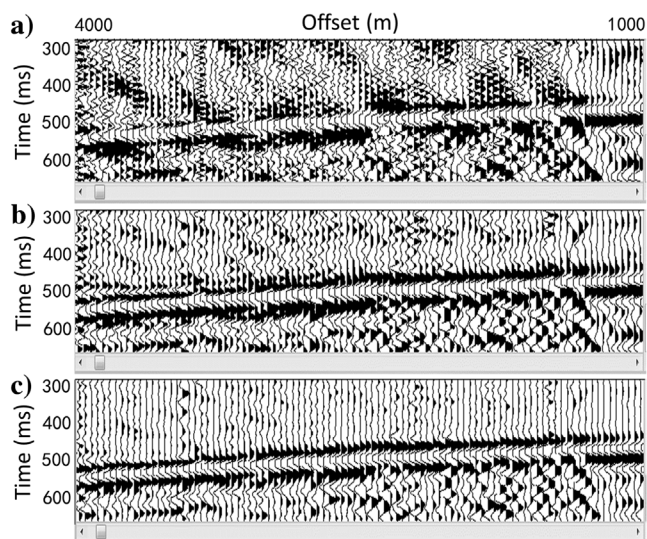
### Near-surface velocity estimation

Near-surface velocity models are estimated by the turning-ray or DWT (Zhu et al., 1992; Bell et al., 1994; Stefani, 1995; Zhang et al., 2006), using the picked first arrivals as discussed in the previous section. A reliable depth of the estimated velocity model from topography is approximately 1/8 to 1/4 of the maximum offset (Figure 13), depending on the materials deposited near the surface. In the KeShen structure (Figure 3, second from right as labeled), the reliable depth is approximately 1/6 of the maximum offset (8000 m) in areas where no thick (>200 m) high-velocity conglomerate rocks are present near the surface; it is 1/10 or less in DaBei and BoZi structures (Figure 3, left) where thick conglomerate

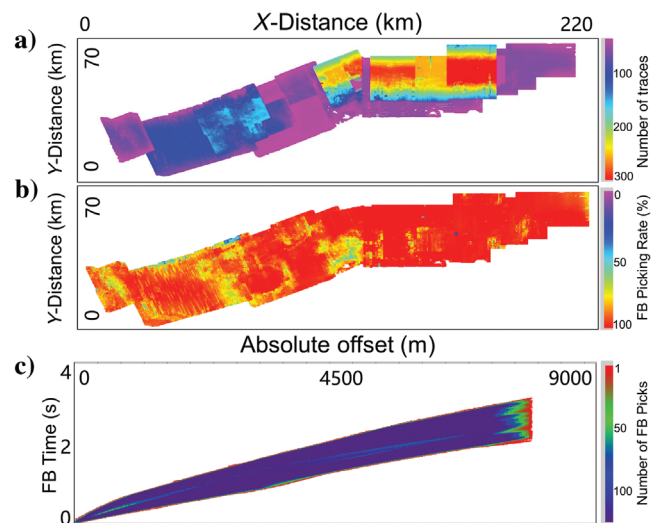
rocks (>400 m) are abundant. Conglomerate rocks are formed from alluvial fans, and they are episodically deposited from the surface (Wang et al., 2013). The velocity in conglomerate rocks depends on the degree of consolidation and grain size. Very often, there is a velocity reversal within a conglomerate-rock column. It is found that the grain size is larger in the shallower section than the deeper section, and it is thickening from east to west (Wang et al., 2013), almost proportional to the height of the mountains (Figure 3).

In turning-ray tomography, the medium to be imaged is generalized into a (gridded) continuous medium, such that the first arrivals recorded at the surface need not be associated with refractors having strong velocity contrasts (Figure 13). Tomographic inversion involves solving a system of linear equations  $\mathbf{t} = \mathbf{D}\mathbf{S}^T$ , where  $\mathbf{t}$  is a column vector of length  $m$  containing observed traveltimes for  $m$  rays;  $\mathbf{D}$  is an  $m \times n$  matrix of ray segments; and  $\mathbf{S}$  is a column vector of length  $n$ , containing unknown slownesses. The objective function  $dt = |T_{\text{cal}} - T_{\text{obs}}|$  is to minimize the difference ( $dt$ ) between the observed or picked first arrivals ( $T_{\text{obs}}$ ) and the calculated or modeled first arrivals ( $T_{\text{cal}}$ ) (Figure 14). Turning-ray tomography is a nonlinear inversion problem. An initial velocity model is required to define raypaths for velocity perturbation, and velocity changes define new raypaths. Convergence requires velocity changes and ray-path updates to be stationary (Figure 14). In general, nonlinear inversion is independent of starting models that are close enough to the actual velocity model.

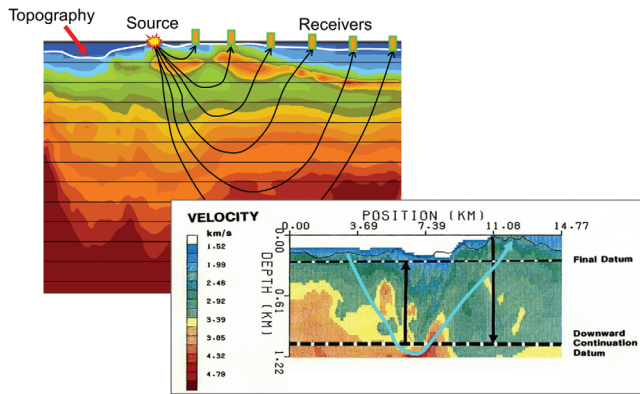
As shown in Figure 9, the quality of the first arrivals is usually better at near offsets and worse at far offsets. This is because of the longer travel distances with more noise contamination and waveform changes at far off-



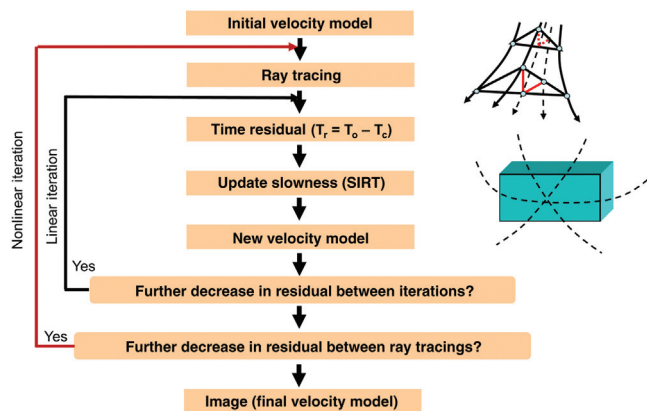
**Figure 11.** Application of the shaping filter (Yu, 1996) before picking the first arrivals of vibroseis data. (a) Original FBs of vibroseis data, which have long-lasting side lobes of waveforms; (b) band-pass filtering is applied to (a) and (c) shaping filtering is applied to (a). The S/N of the first arrivals after shaping filtering has been greatly improved.



**Figure 12.** Quality control of FB picking. (a) The number of traces of 16 3D surveys from the Kelasu task force, where the red and yellow colors represent high numbers and the blue and purple are low numbers, (b) the FB-picking rate, where the red and yellow are high and the green and blue are low, and (c) FB-times versus the absolute offset. The total area of the 3D surveys is approximately 9000 km<sup>2</sup>.

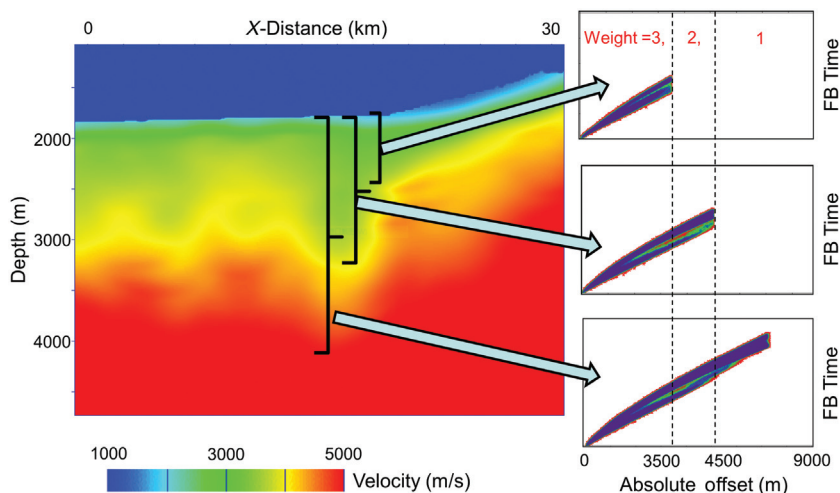


**Figure 13.** Concept of turning-ray tomographic inversion and tomostatics (modified from Zhu et al., 1992). Once a near-surface velocity model is estimated by turning-ray tomography, static corrections are performed by downward and upward (vertical) continuation, downward using the model velocities and upward using a constant-replacement velocity. The downward continuation datum usually is defined as a flat subsurface, a surface subparallel to the topography or the base of the low-velocity layer. The final datum usually is flat and consistent with that defined in time processing.



**Figure 14.** A workflow showing nonlinear turning-ray tomographic inversion (modified from Zhu et al., 1992).

**Figure 15.** Iterative weighted near-surface tomography. First, full-offset first arrivals are used to produce an initial model; second, the initial model is used for the next inversion, using offsets from zero to a middle range; finally, near-offset first arrivals are used to produce a final velocity model. This is equivalent to a weighted tomography in which the near-offset FBs have been used three times whereas the far-offset FBs have been used only once.



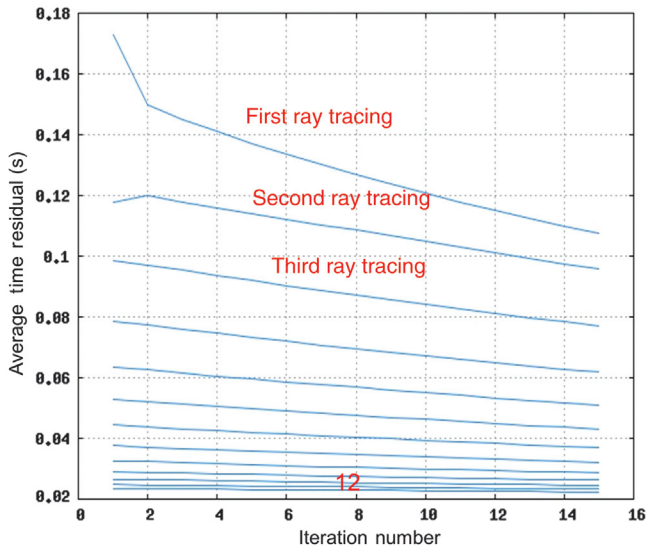
sets. Therefore, we applied a weighted tomography (Figure 15), giving higher weights to the near offsets to recognize the contributions of the near-offset first arrivals to tomography. This has improved the accuracy of velocity model in the shallow section and sped up convergence in the inversion. Some artifacts, such as abnormal boundaries and low-velocity clusters found from the equally weighted tomography, have been removed from the variable-weighted tomography.

Figure 16 shows the convergence curves of the nonlinear weighted tomographic inversion for the entire Kelasu 3-blocks of first-arrival traveltimes containing 16 3D surveys, using full offsets from 0 to 9000 m. The time residual decreased from 180 ms in the beginning to 22 ms at the end, which indicates that the inversion is convergent. The grid size used in inversion is  $15 \times 15 \times 10 \text{ m}^3$  in the inline, crossline, and depth directions. Consequently, the total model size for inversion for the entire Kelasu surveys is  $14,047 \times 5001 \times 501$  in the inline, crossline, and depth directions, respectively. To carry out the inversion for such a large model size, we implemented parallel computing using OpenMP within a node and message passing interface (MPI) between nodes. In total, 10 nodes were used, and each node contained 768 GB memory. A regularization filter or smoothing operator was applied during the inversion to remove numerical artifacts caused by null spaces.

After near-offset first arrivals are inverted to produce a near-surface velocity model, static corrections are performed by downward and upward (vertical) continuation, downward using the model velocities and upward using a constant-replacement velocity for all surveys. In the mega-survey, the near-surface model depth varies because the different subsurveys have low-velocity layers

of different depths (Figure 17). A constant final datum is fixed for all surveys.

The near-surface velocity model is used in a joint or integrated tomography for the subsequent velocity model building for PSDM. In the joint tomography, the near-surface velocity model is merged with a legacy velocity model, such as a velocity model previously used in the legacy PSDM. At the suture zone of the merge, tapering is applied to avoid abrupt velocity changes. Because the near-surface velocity-depth model derived from turning-ray tomography is more accurate and has higher resolution than that from reflection tomography beneath the surface, we keep this model unchanged during the early stages of iterations in the integrated



**Figure 16.** Convergence curves of nonlinear tomographic inversion for the entire Kelasu 3D surveys. Parallel computing was performed using OpenMP and MPI. Each nonlinear inversion represents a ray tracing based on the updated velocity model.

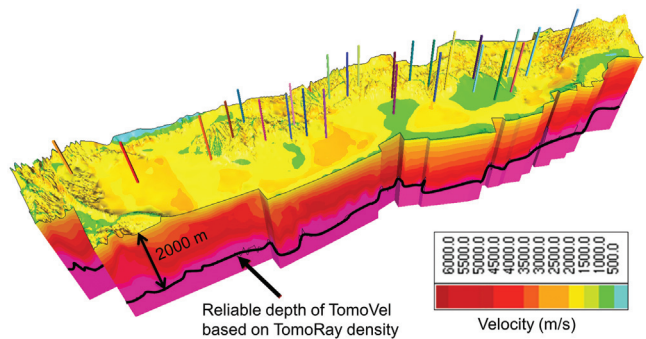


**Figure 17.** Volumetric display of the Kelasu near-surface velocity model estimated from turning-ray tomography. The maximum offset used is 9000 m. Based on the ray density, the maximum reliable depth varies from a few hundred meters in areas with conglomerate rocks to 2000 m in areas without conglomerate rocks. More than 100 VSP data are available (as shown in the vertical bars) for calibration. Although the actual size of 3D surveys is approximately 9000 km<sup>2</sup>, the total size for tomographic inversion is close to 15,000 km<sup>2</sup>.

tomography. To account for the errors associated with the picked first arrivals for turning-ray tomography and combine both models seamlessly, we allow reflection tomography to update shallow and deep velocities simultaneously in the later stage of iterations (Tian et al., 2018). Reflection tomography is a global inversion. At early stages of model building, errors in estimation of models are larger in deeper areas than in shallower areas. The errors in deeper areas affect shallower areas. To avoid error transfer to the near-surface model derived by the turning-ray tomography, the near-surface model is masked in the first several iterations. After a few iterations of reflection tomography, the errors are reduced. Then, reflection tomography updates the velocity and anisotropic parameters in shallower and deeper areas.

## Results

Final tomographic velocity inversion results and their applications to statics and PSDM are illustrated in Figures 17–28.

Figure 17 shows the near-surface velocity volume of the Kelasu structure. Rough topography and strong lateral velocity variations are evident. Representative wells displayed in Figure 17 are used for calibration between vertical seismic profile (VSP) compressional wave (P-wave) velocities and tomographic velocities (TomoVel). The maximum reliable depth of the estimated near-surface velocities is indicated by the bottom of the ray density (the black line) based on the final step of nonlinear inversion, and each nonlinear inversion is performed by ray tracing using the updated velocity model (Figure 14).

Figure 18 illustrates tomographic velocity-depth slices 120 and 500 m below and parallel to the topography, respectively. The shapes of high-velocity geobodies on TomoVel, representing conglomerate rocks, are consistent

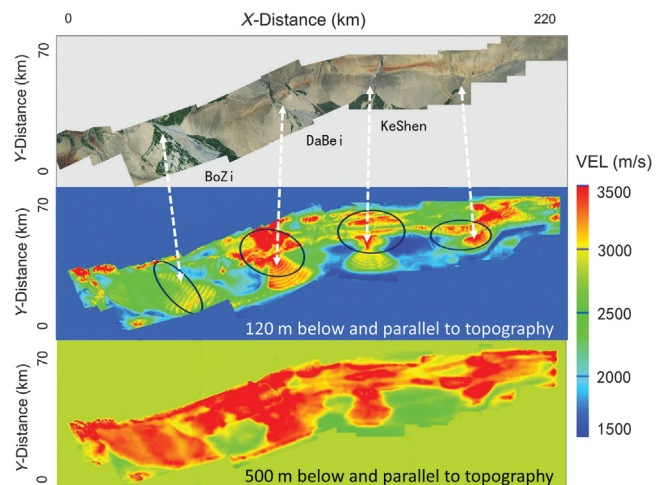


**Figure 18.** Velocity-depth slices 120 and 500 m below and parallel to the topography. The patterns of high-velocity conglomerate rocks with circles estimated from near-surface tomography are consistent with the satellite landscape. Note that the root of the alluvial fans, as circled containing the larger grain size of conglomerate rocks, is associated with higher velocities.

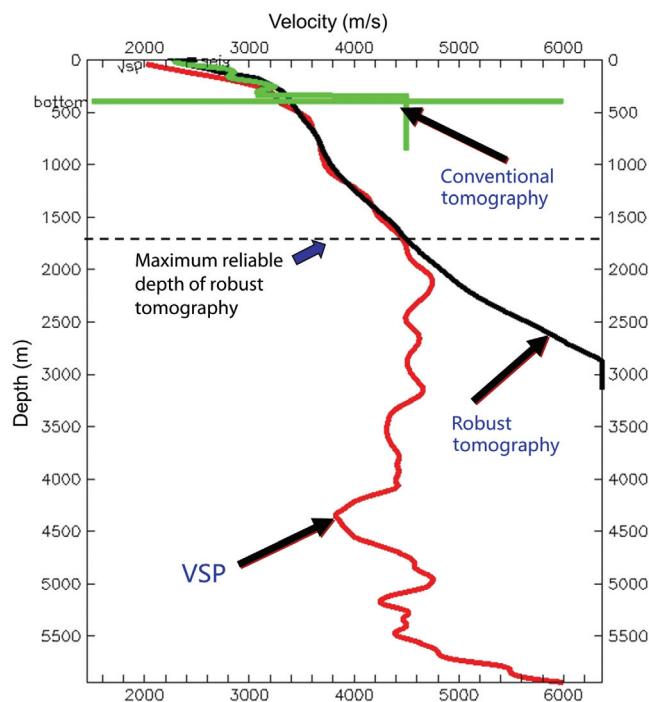
with the primary surface geology structure from satellite landscape, the alluvial fans. The velocities near the root of the fans are higher because the grain size of the conglomerate rocks at the root usually is larger.

In tomographic inversion, we did not use shallow-hole micrologging data as a constraint, as they frequently cause “bull’s-eyes” anomalies. The shallow-hole micrologging surveys provide a velocity depth of only a few meters to a few hundreds of meters, and the velocities converted from the micrologging usually are different from the surrounding TomoVel. Instead, we applied calibration after the inversion, using a single function from more than 60 VSP data in the study area. Those VSP data were reprocessed and evaluated with good quality, especially in the shallow section. It is a depth-variant calibration. Figure 19 shows a comparison between KS3 VSP and TomoVel after calibration. The agreement between the two is excellent.

Conventional turning-ray tomography or DWT using near-offset first arrivals can estimate only a very shallow velocity model for static corrections (Figure 15). We used a robust turning-ray tomography (Zhu et al., 1992, 2008), which can estimate a much deeper near-surface velocity model using full-offset first arrivals for PSDM from topography (Figure 20).

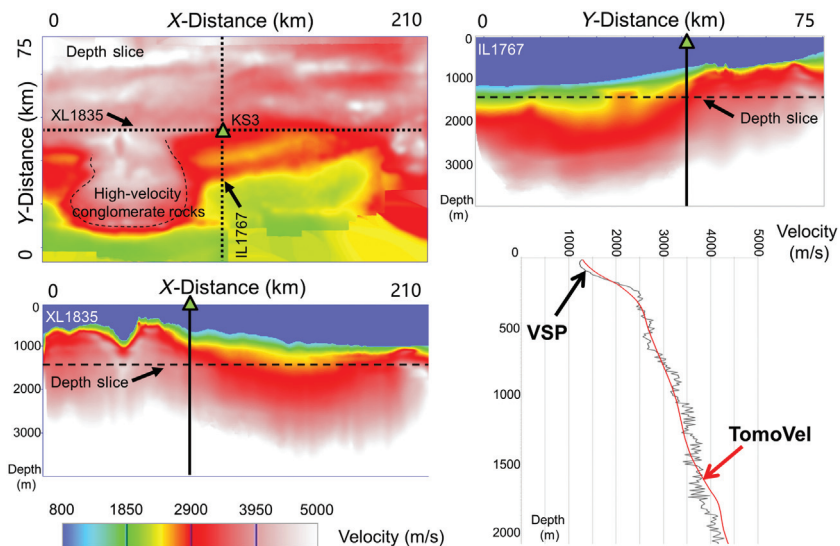
More than 60 VSP data were evaluated in areas with and without high-velocity conglomerate rocks. Representative interval and average velocity comparisons are shown in Figure 21a and 21b. The goodness of fit is approximately 67% and 90% for areas with and without conglomerate rocks, respectively. The reason for the lower goodness of fit in areas with conglomerate rocks is that a velocity reversal occurs in the middle of the conglomerate-rock column as shown in Figure 21a (right) by the arrow. Starting from the velocity-reversal point, rays travel downward (Figure 22). Only when hitting a higher velocity layer in a deeper section due to compaction of rocks will the rays turn back to the surface at a longer offset (Grant and West, 1965). This

produces a shadow zone (Figure 22) or “hidden layer” where refraction inversion is unreliable. For this reason, estimating velocities below the high-velocity conglomerate rocks is not easy by turning-ray tomography using the first-arrival traveltimes as input data. Full-waveform inversion may have a better chance to get a slightly deeper velocity profile with a finite-frequency band, but it is still limited by the recording aperture. Instead, we highly recommend that a joint tomography,



**Figure 20.** A comparison between the conventional turning-ray tomography (DWT) using offsets up to 3500 m and the robust turning-ray tomography using offsets up to 9000 m. The maximum reliable depth of TomoVel in areas without conglomerate rocks is approximately 400 and 1500 m with conventional tomography and robust tomography, respectively.

**Figure 19.** VSP and TomoVel calibration at well KS3. The depth slice is at 1450 m below the highest elevation. The VSP and TomoVel are displayed from the surface.



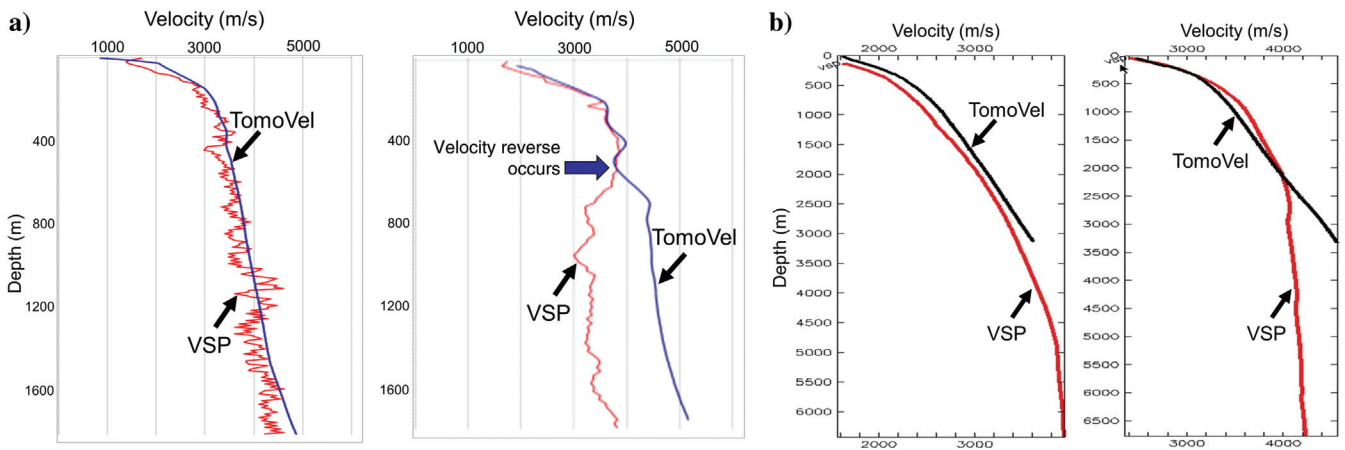


**Figure 21.** (a) Representative interval VSP velocity and TomoVel in areas without conglomerate rocks (left) and with conglomerate rocks (right). Based on more than 60 VSP data, the goodness of fit is approximately 67% in areas with conglomerate rocks and 90% without conglomerate rocks. (b) The representative average VSP velocity and TomoVel in areas without conglomerate rocks (left) and with conglomerate rocks (right).

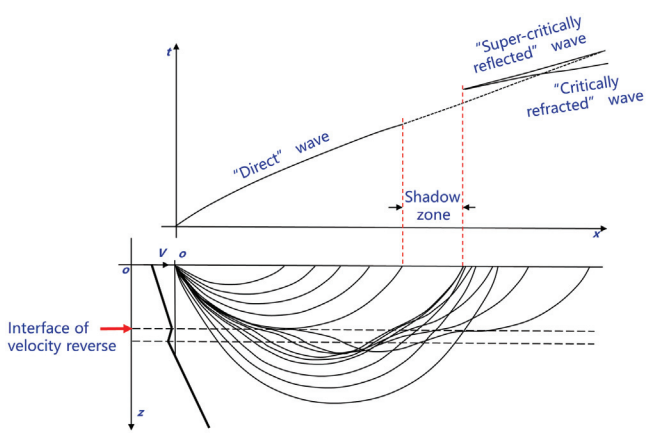


**Figure 22.** The formation of a shadow zone by a region of decreasing velocities. (After Grant and West, 1965.)

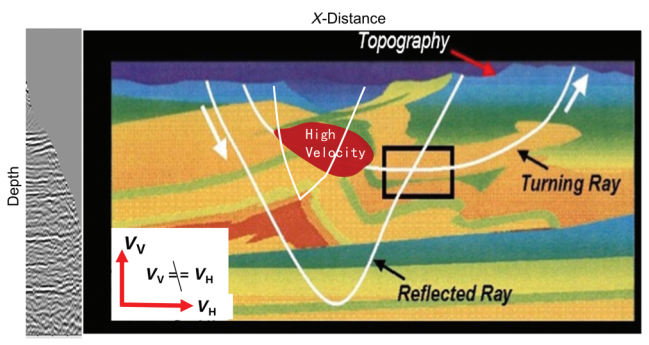


**Figure 23.** An early concept of joint refraction and reflection tomography (modified from Zhu et al., 2001, 2003). Reflection tomography usually is good at estimating velocities in the deep section but not in the shallow section due to the limited offsets of the events. In contrast, turning-ray or refraction tomography usually is good at estimating velocities in the shallow section but not in the deep section due to the limited offset of the input first arrivals. Combining the two can produce a velocity model good at shallow and deep sections.

using refraction and reflection data (Figure 23), be used to get a whole velocity model for PSDM from topography in foothills exploration areas (Tian et al., 2018).

Representative static corrections and PSDM using velocities estimated from turning-ray tomography are shown in Figures 24–26. In statics estimation, the first arrivals up to 3500 m offset were used for tomography because statics calculation requires velocities only at a

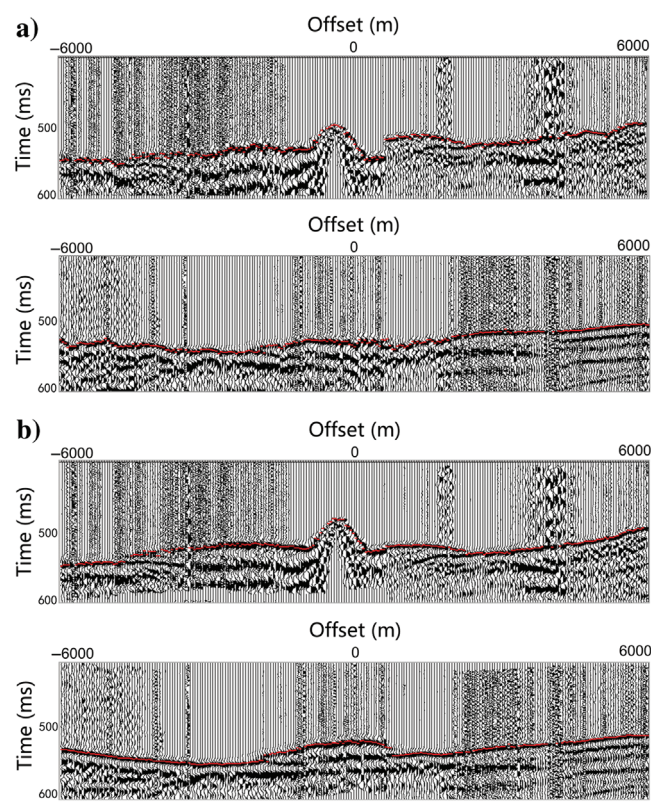


**Figure 24.** (a) Two representative raw shot records with LMO. (b) Two representative shot records after tomostatics with LMO.

shallow depth, usually less than 300 m. The improvement in the first and later arrivals after tomostatics is evident (Figure 24).

In PSDM, full-offset (0–9000 m) first arrivals were used for tomography, aiming at a deeper penetration of the rays. The shallow-velocity model estimated from turning-ray tomography was first merged with a legacy deep-velocity model, usually from a previous study, followed by tapering the suture zone to avoid abrupt changes when updated by a joint refraction and reflection tomography. The preliminary PSDM results already have shown improvement in the shallow section with the help of near-surface velocities estimated from turning-ray tomography in the Kelasu foothills (Figure 25). Results from updating the deeper velocity model will be shown in a future paper.

Figure 26 shows a comparison between PSDM stacks previously imaged from 16 individual surveys (Figure 26a) and recently imaged based on the combined surveys from the task force (Figure 26b) for an arbitrary northeast–southwest line in the Kelasu foothills. Differences and imaging boundaries between the surveys in Figure 26a have been minimized in Figure 26b, leading to better interpretation and reservoir characterization.

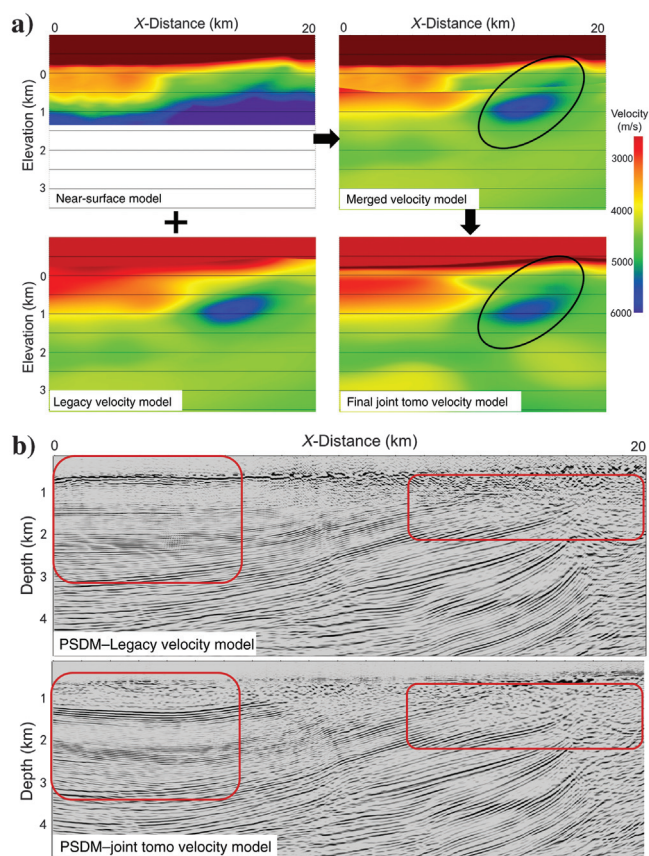


**Figure 25.** (a) Velocity model building for PSDM. The shallow-velocity model estimated from turning-ray tomography was merged with a legacy velocity model, followed by smoothing the suture zone and updated by a joint refraction and reflection tomography (Tian et al., 2018). (b) PSDM results using the legacy velocity model (top) and the joint-tomo model (bottom).

Although VSPs frequently are used for calibration with velocities estimated from tomography, the difference between VSP velocities and TomoVel usually are large. This is because (1) VSP raypaths are almost vertical whereas turning-ray tomography raypaths contain a substantial horizontal component and (2) VSP velocity measurement is dependent upon a dipping layer along a specific azimuth (e.g., northeast–southwest in Figure 27), whereas TomoVel is a summation of estimates from all azimuths. Therefore, VSPs should be used with caution in calibration. Very often, TomoVel using the first arrivals selected from the same azimuth sector as that of VSP measurement match the VSP velocities the best (Figure 27e). Given a measured traveltime  $T$ , the interpreted VSP velocity ( $V_1$ ) usually is larger than the interval velocity ( $V_2$ ) when the layers are dipping along a specific azimuth because the distance  $DH$  along raypaths is larger than the bed thickness  $DZ$  (Figure 27c).

Another interesting observation is that the ray-density plot from the turning-ray tomography (TomoRay) can be used to assist characterization of the top and base of conglomerate rocks, and possibly the velocity-reversal point (Figure 28). This is because rays will be turned or bent at a sharp velocity boundary (Figure 22), forming abnormal ray density at the interfaces. Velocity interfaces showed in VSP (Figure 28) are consistent with the tomographic ray density spikes at a specific location, indicating that the TomoRay is sensitive to the velocity gradient and is useful information for identifying the top and base of the conglomerate rock columns. We expect that an integrated study, using TomoVel, the TomoRay, satellite landscape, and near-surface geology as well as electromagnetic measurements, will help us better understand the conglomerate-rock distributions for seismic imaging and drilling engineering.

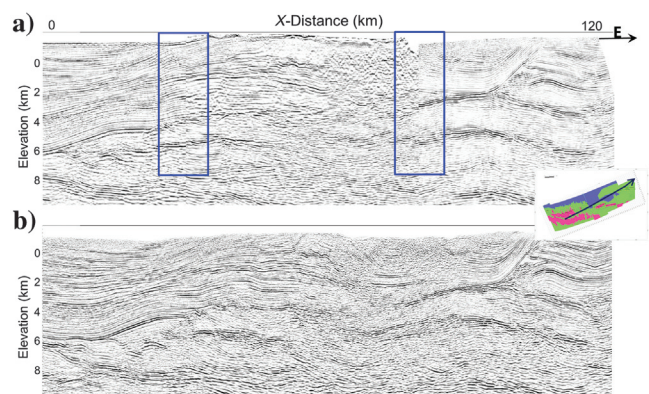


**Figure 26.** A comparison of PSDM stacks from individual surveys and combined surveys for an arbitrary northeast–southwest line. (a) PSDM imaging from 16 individual surveys and (b) PSDM imaging from the combined surveys as a result of the task force. The processing differences and imaging boundaries (as shown with the blue blocks) between the surveys in (a) have been reduced in (b), leading to better interpretation and reservoir characterization.

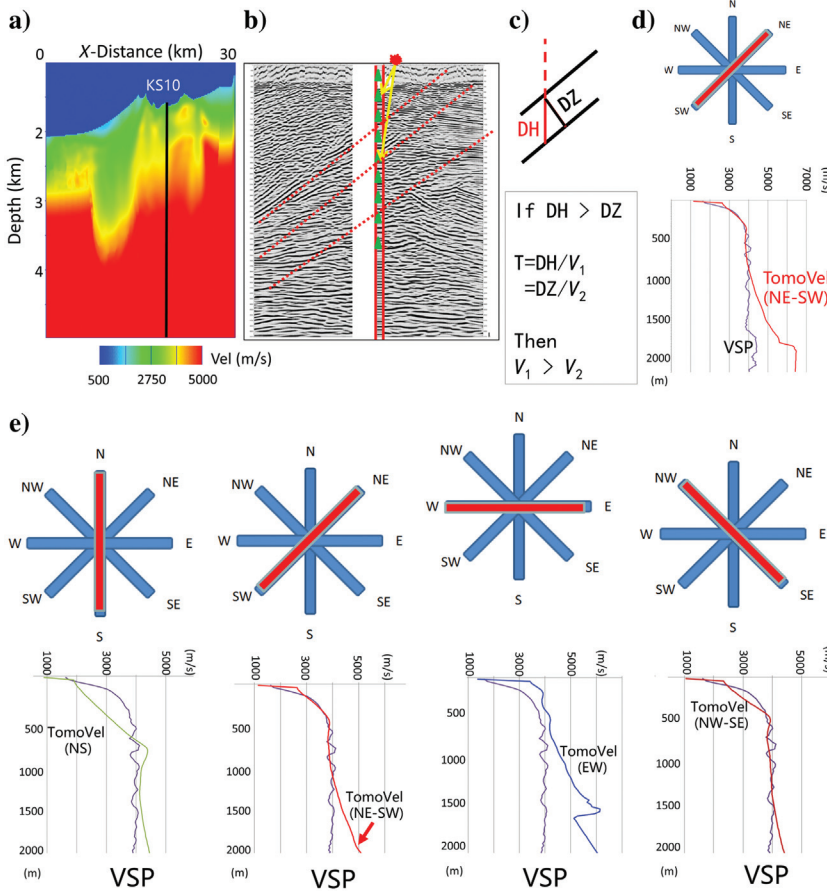


**Figure 27.** Integrated VSP and azimuthal near-surface velocity analysis. (a) Near-surface TomoVel estimated along the northeast–southwest sector of the first arrivals, (b) VSP corridor stack, the VSP raypaths in yellow (almost vertical) and dipping layers in the dashed red lines, (c) a diagram showing that the VSP velocity ( $V_1$ ) is larger than the interval velocity ( $V_2$ ) when the layers are the dipping along a specific (northeast–southwest) azimuth, (d) the VSP velocity ( $V_1$ ) agrees with TomoVel best when TomoVel was estimated along the northeast–southwest direction, matching the structural orientation, and (e) comparisons between VSP velocities and TomoVel estimated from the first arrivals selected from various azimuthal sectors.

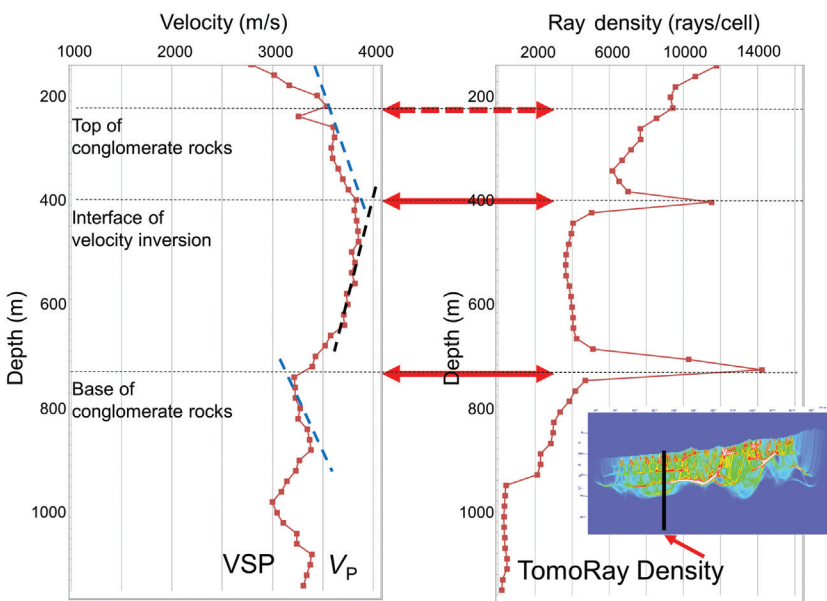


**Figure 28.** Illustration of integrated studies using VSP, TomoVel, and TomoRay for characterizing conglomerate rocks.

**Conclusion**

We have presented an innovative approach to solving a matrix of blocks and tasks in foothills imaging. Successful applications of this approach to Kelasu

foothills have demonstrated that it is a current best practice for a long-run foothills program in a study area. The principal conclusions are:

- 1) The present megaproject is a merge of several 3D surveys in foothills areas, with the merge performed

in a coordinated, systematic fashion in contrast to most land megaprojects. Creative project management is one of the keys to success for the proposed novel strategy. Under the good coordination provided by the oil company, a matrix of blocks and tasks was solved effectively. This success is applicable to most other parts of the world, such as North and South America, the Arabian Peninsula, and North Africa, where near-surface and subsurface conditions are complicated.

- 2) Quality control is another key to success for near-surface velocity estimation and static corrections. Although zero crossing is recommended for picking the first arrivals of dynamite data, it is not adequate when the near-surface lateral-velocity variation is strong and the S/N of the first arrivals is low. Very often, the automatically picked zero crossings cannot follow the up and down shape of the first arrivals. In this scenario, we recommend to first pick the peaks of the first arrivals and then to move them to the zero crossings. Because of the frequency variations at near and far offsets and the lithology and attenuation differences near the surface, a statistical approach should be used to estimate time-shift values from peaks to zero crossings at different offsets. Usually, several statistics models are necessary for different blocks in a megasurvey.
- 3) The near-surface velocity model has a large effect on imaging deep targets. This was confirmed by this megasurvey project, and it is consistent with previous results (Tian et al., 2018). Weighted tomographic inversion, with more weights at near offsets and fewer weights at far offsets, has produced an accurate near-surface velocity model. Consequently, it results in better imaging after joint tomography and PSDM.
- 4) Picking the first arrivals is the bottleneck for near-surface velocity estimations and static correction. The AI first-break (FB) picking presented in this paper is significant, and it greatly improves the efficiency.

### Acknowledgments

We thank G. McMechan, N. House, A. Bertagne, B. Zhao, Z. Liu, Q. Liu, B. Yang, K. Xu, C. Wang, Y. Pan, L. Qin, Y. Zhang, B. Fang, F. Chen, G. (Yan) Yan, and J. Jiao for the constructive discussions. We also are grateful for the help of G. Lei, Y. Xiao, C. Xiao, X. Wang, R. Zhao, and H. Gao for providing project management support and resources. We thank the Tarim Oilfield Company of PetroChina and Forland Geophysical Services for permission to publish this work. Constructive suggestions and comments from S. Gray, G. Dutta, and two anonymous reviewers are very much appreciated.

### References

Bell, M. L., R. Lara, and W. C. Gray, 1994, Application of turning-ray tomography to the offshore Mississippi delta: 64th Annual International Meeting, SEG, Expanded Abstracts, 1509–1512, doi: [10.1190/1.1822824](https://doi.org/10.1190/1.1822824).

- Cox, M., 1999, Static corrections for seismic reflection surveys: SEG References No. 9, 531, doi: [10.1190/1.9781560801818](https://doi.org/10.1190/1.9781560801818).
- Grant, F. S., and G. F. West, 1965, Interpretation theory in applied geophysics: McGraw-Hill.
- Gray, S., and X. Zhu, 2019, Foothills seismic imaging challenges: Past, present and future: The 2nd SEG Foothills Exploration Workshop, Chengdu, China, doi: [10.1190/FEW2019-01.1](https://doi.org/10.1190/FEW2019-01.1).
- Song, M., X. Liu, X. Han, D. Wang, S. Yang, and C. Hinz, 2014, Combining diving-wave tomography and prestack reflection tomography for complex depth imaging — A case study from mountainous western China: The Leading Edge, **33**, 868–874, doi: [10.1190/tle33080868.1](https://doi.org/10.1190/tle33080868.1).
- Stefani, J. P., 1995, Turning-ray tomography: Geophysics, **60**, 1917–1929, doi: [10.1190/1.1443923](https://doi.org/10.1190/1.1443923).
- Taner, M. T., A. J. Berkhout, S. Treitel, and P. G. Kelamis, 2007, The dynamics of statics: The Leading Edge, **26**, 396–402, doi: [10.1190/1.2723200](https://doi.org/10.1190/1.2723200).
- Tian, J., G. Peng, J. Jiao, G. Yan, and X. Zhu, 2018, Integrated turning-ray and reflection tomography for velocity model building in foothill areas: Interpretation, **6**, no. 4, SM63–SM70, doi: [10.1190/INT-2018-0005.1](https://doi.org/10.1190/INT-2018-0005.1).
- Wang, Z., D. Zhong, H. Sun, H. Yang, H. Xie, Y. Li, G. Lei, X. Yang, Q. Wu, and B. Zhang, 2013, Sedimentary characteristics and distribution of neogene-quadernary gravel layers in the middle of Kuqa depression, Tarim basin: Acta Sedimentologica Sinica, **33**, 282–286, doi: [10.1016/j.chnaes.2013.07.008](https://doi.org/10.1016/j.chnaes.2013.07.008).
- Yu, S., 1996, Wide-band Ricker wavelet: Petroleum Geophysical Prospecting, **31**, 605–615.
- Zhang, J., O. Yilmaz, and N. Dai, 2006, First-arrival tomostatics and residual statics for near-surface corrections: CSPG-CSEG-CWLS Convention, 317–321.
- Zhou, C., J. Jiao, S. Lin, J. Sherwood, and S. Brandsberg-Dahl, 2011, Multiparameter joint tomography for TTI model building: Geophysics, **76**, no. 5, WB183–WB190, doi: [10.1190/geo2010-0395.1](https://doi.org/10.1190/geo2010-0395.1).
- Zhu, X., 2002, Velocity imaging through complex near-surface structures by tomography: 64th Annual International Conference and Exhibition, EAGE, Extended Abstracts, E037.
- Zhu, X., A. Huffman, and J. Castagna, 2003, Tomography for enhanced geopressure prediction and depth imaging: SPG/SEG Conference in Beijing.
- Zhu, X., D. P. Sixta, and B. G. Angstman, 1992, Tomostatics: Turning-ray tomography + static corrections: The Leading Edge, **11**, 15–23, doi: [10.1190/1.1436864](https://doi.org/10.1190/1.1436864).
- Zhu, X., P. Valasek, B. Roy, S. Shaw, J. Howell, S. Whitney, N. D. Whitmore, and P. Anno, 2008, Recent applications of turning-ray tomography: Geophysics, **73**, no. 5, VE243–VE254, doi: [10.1190/1.2957894](https://doi.org/10.1190/1.2957894).
- Zhu, X., K. D. Wyatt, and A. Lau, 2001, Turning-ray tomography and tomostatics: “Recent Advances and the Road Ahead” session at SEG Annual Meeting.



**Yalin Li** is a distinguished professor-level geophysicist and vice president of geophysical operations at PetroChina Tarim Oilfield. He received a B.S. (1986) in petroleum geology from Chengdu College of Geology, an M.S. (1996) in petroleum geophysics from Southwest Petroleum Institute, and a Ph.D. (1999) in petroleum geophysics from Chengdu University of Technology. Li has been engaged in the research of foothills exploration from seismic acquisition to processing, imaging, and interpretation at China National Petroleum Corporation (CNPC) for nearly 30 years. He has managed and implemented over 20 key geophysical research and development (R&D) projects and more than 100 foothills seismic-engineering projects at CNPC. Li is technically responsible for the discovery of numerous important oil and gas reservoirs in complex foothills regions of Western China using advanced geophysical methods, and he is the winner of China National Technology Invention Award. He has published more than 60 technical papers, and obtained more than 20 invention patents and 20 software copyrights.



**Xianhuai Zhu** has more than 30 years of both oil and service company experience. After receiving his Ph.D. (1990) in geosciences from the University of Texas at Dallas, he worked with Anadarko, PGS, and ConocoPhillips. In 2016, Zhu founded Forland Geophysical Services Company (FGS) in Houston, developing and applying advanced imaging technologies For Land. Zhu received a Reginald Fessenden Award from SEG in 2012 for his pioneering work on turning-ray tomography and tomostatics, and a Life Membership Award from SEG in 2018. In 1999, he received the Best Paper Award from SEG on "Recent advances of multi-component processing." Zhu served as a director-at-large on the SEG Board of Directors from 2014 to 2017 and the first vice president of Geophysical Society of Houston (GSH) from 2017 to 2018.



**Gengxin Peng** is a professor-level senior engineer and distinguished geophysical expert at PetroChina Tarim Oilfield Company. He has been engaged in seismic data processing and interpretation research and technology control in Tarim for 30 years and has participated in and undertaken many major research projects from the Chinese government and PetroChina. He has won 10 awards at or above the provincial level, seven national technical invention patents, three coauthored monographs, and has published more than 30 papers.



**Liansheng Liu** received his M.Sc. (1993) in geophysics from Chang'An University (P.R. China) and then joined BGP for seismic data processing and research and development. He established PanImaging Software Development LTD in 2004. Liansheng is the main developer of ToModel which is being widely used for solving near surface problems for land seismic exploration. He was awarded the National Science and Technology Progress Award in 2003.



**Wensheng Duan** is a senior expert of CNPC. He received his doctorate (2013) from China University of Geosciences (Beijing). He has worked for Tarim Oilfield Company, PetroChina for more than 28 years. He has engaged in seismic data processing and made great contributions to the popularization and application of OVT techniques in China. He made some academic achievements, not only publishing 30+ papers but also winning 10+ distinguished awards.